Algorithms for a Fast Confocal Optical Inspection System

A. R. Rao, N. Ramesh, F. Y. Wu, J. R. Mandeville,
I.B.M. Research Division
T. J. Watson Research Center
Yorktown Heights, N.Y. 10598

and P. J. M. Kerstens
I.B.M. General Technology Division
Rt. 52, Hopewell Jct.
N.Y. 12533

Abstract

Confocal imaging is an emerging technique for the measurement of surface topography in inspection. In this paper we present a system designed for fast acquisition and processing of confocal images, which consists of an optical front end using tilted confocal scanning, and an image processing module.

The function of the image processing module is to improve signal resolution, perform smoothing and detect surfaces in the incoming signal. The input signal is first deconvolved in order to improve the depth resolution, and then processed to identify significant peaks. These peaks represent the position of different surfaces in the object being inspected. These peak locations are smoothed using a cluster based smoothing scheme to combat noise. For semi-transparent materials, our system is capable of detecting up to two surfaces at a given location.

1 Introduction

The measurement of surface topography is an important requirement in many manufacturing processes. Some of the techniques developed include laser triangulation [1], SEM stereo [2], SXM [3] and stylus profilometry. Another technique which is receiving increasing attention is based on the confocal microscope.

A confocal microscope can be used to generate a high resolution image of a thin slice of a thick object [4]. In contrast to conventional two dimensional microscopy, confocal microscopy allows one to generate a three dimensional image by optically scanning a point source and a point detector across the object.

The advantages of confocal imaging lie in its non-contact measurement, high speed operation (greater than 10 megapixels/sec), submicron resolution, and the provision of height information in multi-layered semi-transparent materials. Currently most confocal imaging systems are used in biomedical imaging [5]. In this paper we discuss the special challenges of using confocal imaging in a manufacturing environment.

Confocal imaging generates multiple optical slices of a translucent object at different planes. However, the image may be blurred due to the presence of other translucent or opaque interfering surfaces and scattered light. Image processing techniques are necessary to filter out extraneous signals to obtain clearer images.

1.1 The role of confocal imaging in inspection

Current products in semiconductor manufacturing are formed of multilayered structures, as shown in figure 1. These layers consist of both opaque (e.g. metal) and transparent materials (e.g. polyimide) that are sandwiched together. The 3D measurement of these structures is an important part of process control and quality assurance. Furthermore, due to the multilayered nature of structures, it is not possible to get a single well focussed 2-D intensity image using a conventional microscope (parts of the image will appear blurred). The confocal microscope can generate a 2-D image that is well focussed at every point.

In biological applications the data in all of the image slices may be significant because frequently the object contains continuous distributions of matter that fluoresce, scatter, or absorb the incident light [5]. However, in the inspection of manufactured electronic parts, there are typically only one or two interfaces at or near the top surface that need to be inspected. The raw confocal image slices contain much more data than is needed for inspection. Consequently a preprocessing step which extracts the heights of the surfaces from the input data should be used to feed the inspection algorithms that check heights, linewidths, pattern accuracy, etc. against design data.

The trend in the semiconductor and packaging industry is towards smaller linewidths and denser circuitry, which places demands for higher throughput, resolution and accuracy in the inspection systems, both for image acquisition and analysis. This fact,

0-8186-2840-5/92 $03.00 © 1992 IEEE

combined with the earlier observation that the confocal images have to be used by inspection algorithms imply stringent speed requirements. For instance, if the confocal microscope is operated at 10 megapixels/sec to produce 16 slices, then we require a processing speed of 160 megapixels/sec. The requirement of high speed limits the choice of algorithms, as discussed later.

2 Principles of operation

The basic principle exploited by the confocal microscope is that of defocus. When a conventionally imaged object is displaced from best focus, the image contrast decreases, but the spatially averaged intensity remains the same. However in a confocal imaging system, the image of a defocused surface appears *darker* than if it were in focus. Thus the confocal optics can be said to have axial resolution in addition to lateral resolution. As a consequence of this property, it is possible to extract topographic information from a set of confocal images taken over a range of focal planes. Figure 2 illustrates the principle.

In a reflective confocal system, a point light source is imaged onto the object. Light reflected from the object and collected by the lens is re-imaged via a beamsplitter onto a point detector. When the object is in the focal plane of the lens, there is a maximum amount of light received by the point detector. When the object is defocused, the reflected light is spread out at the detector, and relatively little is received by the point detector. For an ideal lens and a mirror-like object, the dependence of detected signal on defocus can be expressed as $I(z) = I_0 sinc^2(\pi \mathrm{NA}^2/\lambda z)$ where $I(z)$ is the light intensity along the axial direction, NA is the numerical aperture, λ is the wavelength, and $sinc(x)$ stands for $sin(x)/x$. The peak signal occurs when the object is in the focal plane, $z = 0$.

In order to form a confocal image, the signal is recorded as the object is scanned relative to the image of the point source in a plane parallel to the focal plane. Multiple confocal image slices are obtained by repeating the process at various levels of object defocus. Thus by focusing at different heights (along the $z - axis$) on the object, it is possible to obtain a 3-D topographical map of the object.

Confocal image processing must solve the inverse problem of determining the surface height(s) from a series of confocal images with varying defocus. The result is a map of the 3D topography of the object.

2.1 The confocal optical system

The system described here is intended to adapt the 3-D imaging properties of confocal optics to automatic inspection. As described above, a confocal system images only one point at a time. Acquiring a complete two-dimensional image requires that either the illuminated spot or the object be scanned in two dimensions. Acquisition speed can be increased by illuminating and imaging multiple isolated spots simultaneously.

The imaging system used in this work is intended for automatic optical inspection of electronic packaging, in which the areas to be inspected are much larger than the field of view of any real optical system capable of the necessary resolution. Consequently in this system, the object is moved across the field of view in a continuous motion as confocal image data are acquired. We acquire multiple images at different focal planes simultaneously by tilting the object and its scanning stage so that the nominal object surface is not normal to the optical axis, as shown in figure 3.

For our application, we use the microscope to acquire a set of 16 confocal images, each at a different focal plane near the top surface of the object. Thus each pixel is associated with 16 values from which surface height(s) are to be calculated. The range of the 16 equally-spaced focal planes is selected to match the inspection requirements.

Figure 4 illustrates the coordinate system that we will use. Imaging from the top, we obtain sixteen slices ($x - y$ plane) of the object along the z direction.

2.2 Considerations arising from manufacturing requirements

The main thrust of our research is to develop fast, accurate and reliable algorithms for height processing. Several issues need to be considered here.

(1) Processing speed is one of the most important requirements in inspection, and is even more crucial when the algorithms to be used are for the front end of the system. This is because the front end merely provides good signals, and the additional overhead of other inspection algorithms has to be incurred. Thus, this requirement implies that time consuming iterative algorithms (which may have superior performance in terms of quality) cannot be used.

(2) The object can have multiple layers, some of which may be transparent. This case creates special degradations of the signal.

(3) The microscope(s) can possess varying response functions. Even nominally identical lenses may have different depth responses, which are usually asymmetrical. Thus, the solution should be adaptable to different depth response functions.

(4) The signal is usually noisy, and has to be filtered to get good results. At the same time, one must

be careful not to smooth out small defects. The objective here is not to fit smooth surfaces to the data, but rather reproduce a given surface faithfully so that defects can be found.

(5) The algorithms should be easily translatable into hardware implementations, in order to maximize processing speed.

3 Algorithms for processing confocal images

The different slices imaged by the confocal microscope produce a typical intensity signal, $g(z)$, along the z direction as shown in figure 4. The algorithms we discuss will operate on the signal $g(z)$. Note that $g(z)$ will exhibit a peak close to the location of the surface of the object. Hence, the general approach we use is to detect a peak in the signal obtained at each (x, y) location.

3.1 Peak Detection

The peak detection algorithm should have controllable sensitivity and be computationally inexpensive. Though there are a number of different peak detection techniques available [6], we developed the following simple scheme based on the strength of zero crossings.

In our application, we have to detect up to two surfaces at a given (x, y) point. Furthermore, weak peaks due to noise have to be eliminated. One way of meeting both requirements is to define a peak strength measure for each peak in the signal. A peak is synonymous with a negatively sloped zero crossing (along the positive direction of the z axis), and is identified through a change in the sign of the first derivative. In addition to peaks, we identify valleys in the signal, which are positively sloped zero crossings. Each peak is flanked by a valley on either side, as shown in figure 5. Note that a significant peak is characterized both by its sharpness (magnitude of the second derivative) and by the area under the peak (product of height and width). The area under the peak is a measure of the local energy of the signal. A simple way of combining both these desirable qualities of a peak is to take their product, yielding

$$P(h, w, g_1, g_2) = hw(g_1 - g_2) \qquad (1)$$

where P is the peak strength measure, h and w are the height and width of the peak as in figure 5, and g_1 and g_2 are the gradients on either side of the peak.

Weak peaks in the signal are eliminated through a threshold (set as discussed in section 7.1) and the two surviving peaks with the largest peak strength measure are interpreted as the two surfaces we seek. The elimination of weak peaks is similar in spirit to the elimination of weak edges in edge detection through hysteretic thresholding [7] or the authentication of zero crossings.

Though this simple peak detection scheme works in most cases, it may fail when one is looking at a semi-transparent object. Such an object gives rise to two or more reflections, whose responses may overlap, as shown in figure 6. We now discuss a way of resolving such an overlap.

4 Deconvolution

Ideally, deconvolution (also known as image restoration) [8, 9] will separate close peaks and enable their separate identification.

The signal degradation model most commonly used is given by

$$g(z) = n(z) + \int f(z - \tau)h(\tau)d\tau \qquad (2)$$

where $f(z)$ is the original signal, $h(z)$ is the point spread function of the optical system $g(z)$ is the output signal, and $n(z)$ represents the additive noise term. Here a one-dimensional model is used.

The deconvolution or restoration problem is to recover $f(z)$ in equation 2, given $g(z)$ and $h(z)$. The estimate of the solution is termed $\hat{f}(z)$.

Deconvolution or restoration techniques can be classified into two broad categories: linear techniques and non-linear techniques. Linear methods are concerned with applying a linear filter to the corrupted signal $g(z)$ in order to recover the original signal $f(z)$. Non-linear techniques allow the imposition of additional constraints on the restoration, such as positivity of the restored signal. In contrast to linear methods, non-linear methods are invariably iterative.

Ideally, a full three-dimensional deconvolution should be performed. Even so, such a three-dimensional deconvolution is valid only if the object is incoherent, as in the case of confocal fluorescence imaging. It is not strictly valid in the present application, where the surfaces are coherent reflectors. In spite of these limitations, we have found that acceptable performance can be achieved with a one-dimensional deconvolution, as described below.

4.1 Linear deconvolution techniques

Wiener filtering is in practice the most widely applicable linear deconvolution method [8][pg. 92], and we used the filter described in [10][pg. 434]. Other linear techniques such as regularization can also be used, as described in [11]. The deconvolution filter derived from regularization is very similar to the Wiener filter.

4.2 Non-linear deconvolution

Non-linear deconvolution techniques have superior signal restoration propertie because they make use of additional constraints such as the positivity of the signals [12]. Linear methods are not capable of guaranteeing this constraint.

We implemented non-linear techniques such as the Jansson-Van Cittert scheme [13, 9] and subtractive deconvolution [8][pg. 80]. We found that they gave superior performance, both in terms of the ability to resolve proximate peaks and the ability to contain the amount of ringing in the deconvolved signal. However, improvement in performance comes at the cost of processing speed. Non-linear techniques are invariably iterative and thus unsuited for real-time applications like the one being addressed.

5 System Overview

The block diagram of the system is shown in figure 7. The 1-D signal corresponding to the different slices along the z axis is deconvolved using a linear filter. The peaks are identified to determine the location and nature of the surfaces: only top surface, top and bottom surface (in the case of transparent materials) and no surface.

The two parallel paths shown in the block diagram correspond to imaging the object in green and blue light. By doing so, we exploit the different reflectance characteristics of the object with respect to the different wavelengths of light used. For instance polyimide is transparent in green light, but opaque in blue light. The use of two bands of light in the imaging operations requires an averaging operation to combine the results into a single surface map. This is described in section 6.

6 Smoothing of height images

After deconvolution and peak detection, we extract at most two peaks, say at z_1 and z_2 at a location (x, y) from each channel. Let j denote the channel, where j is either G or B for green or blue. These two peaks are stored in an upper height image, I_{1j}, and a lower height image, I_{2j}, ($I_{1j}(x, y) = z_1$ and $I_{2j}(x, y) = z_2$). We assume that the top surface of the object is positioned in the range of the system. Therefore, if only one peak is detected, it is the top surface, and we encode the lack of a peak with the z-value of 0. If the signal in channel j at location (x, y) contains only one peak at z_1, then $I_{1j}(x, y) = z_1$ and $I_{2j}(x, y) = 0$. If the signal at (x, y) contains no peaks, then $I_{1j}(x, y) = I_{2j}(x, y) = 0$.

Thus each channel produces two height images, giving a total of four: I_{1G} and I_{2G} corresponding to the green channel, and I_{1B} and I_{2B} corresponding to the blue channel. The heights measured at a location (x, y) can be different in the green and blue channels due to noise or systematic offsets, and have to be combined to produce a consistent height. One may expect a pairwise averaging of I_{1G} and I_{1B} to provide an averaged upper surface image, I_1, and averaging I_{2G} and I_{2B} to provide an averaged lower surface I_2.

However, this pairwise averaging does not work because there are two sources of measurement errors. There are minor variations due to noise, and major variations due to the fact that a surface may be detected in one channel but missed in the other. Pairwise averaging fails if there are such missing surfaces.

Hence we need a technique to smooth the four images *simultaneously*. Different methods can be applied here, and we use a clustering technique from the pattern recognition literature [14].

6.1 A clustering approach to smoothing

Since the object contains at most two discernible surfaces at a given (x, y) location, we expect these surfaces to be manifested by two clusters in the z measurements made in the vicinity of (x, y). Conventional clustering algorithms are iterative [14], and hence must be modified before use.

The inter-slice sampling distance is typically chosen such that there is a reasonable separation (two or more samples) between two adjacent surfaces on the object. This implies that the two clusters that may be present are well separated.[1] This fact is made use of in the clustering algorithm.

For each location (x, y), we form a neighborhood of size NxN (N is typically 3 or 5). A histogram of heights z from the four images within this neighborhood is created. and is scanned to identify well separated clusters. The two clusters with the maximum number of data points are selected and the cluster centroids (in z) are taken to be the smoothed height values.

6.2 Resolution of the imaging system

We approach the issue of resolution from the viewpoint of being able to detect a defect in the object. There are two possibilities here: the resolution along the optical axis, and lateral resolution.

6.2.1 Resolution along the z axis

As seen in section 3, surfaces are identified as peaks in the set of slices. Linear deconvolution (section 4) can

[1] If the two clusters corresponding to the two surfaces are close enough to merge, then the resolution limit of the system has been exceeded. This gives rise to interference phenomena described in section 6.2.

separate proximate surfaces only if they are farther than two sample slices apart. Thus, the resolution of our system is limited to the distance between two sample slices. However, defects below this resolution can be detected by alternate means, as follows.

Interestingly, it turns out that if two surfaces are indeed very close together, then interference can be observed in the 2-D intensity image as shown in figure 8. We used an optical simulator package to study this phenomenon, which predicted that interference fringes can be observed for polyimide on metal if the polyimide layer is less than 5 microns thick. These interference fringes could be detected by the back-end inspection algorithms to indicate the presence of the related height defect.

6.2.2 Lateral $(x-y)$ resolution

By lateral resolution we mean the smallest lateral extent of a height defect that the system can detect. The major factor determining the lateral resolution is the size of the window used in surface smoothing. There is a tradeoff between two factors: combating noise and preserving the ability to detect small defects. A larger window gives better immunity to noise, but smooths out small defects.

In our system, the lateral resolution (in pixels) is $\lceil N/2 \rceil$ where N is the number of pixels in the smoothing window.

7 Experimental Results

All the experiments were conducted on an IBM RS/6000 workstation running AIX 3.1.5. We used both synthetic and real images to test our image processing and surface detection algorithms.

7.1 Evaluation Criteria

The performance of the system is a function of the noise level present as well as the particular values selected for thresholds that may be needed. In order to evaluate the system performance, it is necessary to define a ground truth, and check the output of the system with respect to this. Since we did not have a real part whose dimensions were accurately known, we generated synthetic data, and added varying degrees of noise to it.

Three major types of errors were categorized for each surface: (1) Extra surfaces detected, (2) No surface detected where one should have been, (3) Surface was detected but the height was outside the allowable tolerance value.

Tolerance bands were specified for the different error types as follows, based on final product specifications. For example, in the top metal, no pixel should exceed the height tolerance which was 0.5 microns, no extra surface should be detected and not more than 0.1% of the surface should be missing.

1. $h_1 \in [H_1 - \Delta_t, H_1 + \Delta_t], h_2 = 0$ – criteria met
2. $h_1 = h_2 = 0$ – missing surface
3. $h_1 \in [H_1 - \Delta_t, H_1 + \Delta_t], h_2 \neq 0$ – extra surface
4. $h_1 \notin [H_1 - \Delta_t, H_1 + \Delta_t], h_2 = 0$ – exceed height tolerance
5. $h_1 \notin [H_1 - \Delta_t, H_1 + \Delta_t], h_2 \neq 0$ – exceed height tolerance and extra surface

where h_1 and h_2 are the observed heights, H_1 is the correct height, and Δ_t is the allowable tolerance.

7.2 Image generation

The synthetic images were generated from the optical characteristics of of the current imaging system. The set of 16 confocal slices was then created by mapping these different surface types via a mask layout pattern as shown in figure 9.

7.3 Addition of noise

Gaussian noise of 0.0 mean and different standard deviations was added to the images generated to test the behavior of our algorithms and determine the noise level at which the system meets all the design requirements. Figure 10 shows the total of different error types discussed in section 7.1 as a function of noise and the peak measure threshold (section 3.1). This determines the operating characteristic of the system, and is used to set the thresholds at the desired level.

The performance expected from the system is a total error of less than 5% up to a noise level of $\sigma = 5$. This requirement translated to a peak measure threshold of 2500, as this gives rise to the minimum total error in figure 10. The choice of this threshold is not critical, and any value between 2000 and 3000 could be used to provide acceptable performance.

7.4 Results of processing the synthetic image

The following sequence of algorithms was applied: (a) deconvolution through Wiener filtering (section 4.1), (b) peak detection (section 3.1), (c) smoothing using cluster based smoothing over a 3x3 window (section 6.1).

Figure 11 shows the result of processing the synthetic images of figure 9. The result is displayed as two grayscale encoded height images – an upper surface image and a lower surface image. Artificial defects were introduced in the generated images by shifting the top polyimide layer down by a small amount in

two rectangular regions. The system is able to correctly identify these defective regions on the top surface as illustrated in figure 11(c)

7.5 Results of processing a real image

Figure 12 shows a set of 16 confocal images of metal lines. This image shows a two layered metal pattern on top of an insulating layer. Beneath the insulating layer is another metal plane.

Figure 13 shows the result of processing the set of 16 confocal images. These results prove that the system is capable of measuring heights of top surfaces and also of measuring the heights of surfaces under a semi-transparent layer.

Note that the lower height image is somewhat noisy – there are "holes" consisting of black pixels. If the signal is too low at a point (due to attenuation), we do not compute the surface height, but instead encode the pixel as having zero height. The metal film whose surface is being detected here is "grainy", possessing many small regions of low reflectivity. Similarly, the upper height image has flecks of white. This occurs because of spurious peaks detected due to the presence of noise.

8 Discussion

The running time of the algorithm on an RS6000 workstation is 90 seconds for an image containing 256x120x16 pixels, where each pixel is encoded with 8 bits. However, this is an unsuitable architecture for the real time operation of this algorithm. We are investigating the implementation of our algorithm on special purpose hardware. The deconvolution can be viewed as a 16x16 matrix multiply operation. This can be implemented by using commercially available chips such as the TRW TMC2250 which operates at 40 Mhz. The peak detection operation can be implemented using comparators and lookup tables.

9 Conclusion

We demonstrated the feasibility of using confocal imaging to provide three dimensional information in industrial inspection tasks. The advantages of confocal imaging lie in its speed, non-contact operation and its ability to image semi-transparent objects.

We developed an algorithm which involves deconvolution with a linear filter (the Wiener filter) to improve signal resolution in the z direction. Though non-linear filters provide better signal restoration capabilities, they are not feasible for real time applications. The restored signal is then processed to detect peaks which in turn represent the heights of different points on the object. Finally, we use a cluster based smoothing technique to smooth the surface heights.

References

[1] G. West and T. Clarke, "A survey and examination of subpixel measurement techniques," in *Proc. SPIE*, vol. 1395, pp. 456–63, Sept 1990.

[2] A. Kayaalp, A. R. Rao, and R. Jain, "Scanning electron microscope based stereo analysis," *Machine Vision and Applications*, vol. 3, Fall 1990.

[3] H. Wickramasinghe, "Scanning probe microscopy: current status and future trends," *J. Vac. Sci. Technol. A, Vac. Surf. Films*, vol. 8, no. 1, pp. 363–8, 1990.

[4] T. Wilson, "Confocal scanning microscopes," in *Proc. SPIE, Optics in complex systems*, vol. 1319, pp. 460–1, 1990.

[5] S. Paddcok, P. DeVries, J. Holy, and G. Schatten, "On laser scanning confocal microscopy and three dimensional reconstruction," in *Proc. SPIE, Bioimaging and two dimensional spectroscopy*, vol. 1205, pp. 20–28, 1990.

[6] J.Eklundh and A.Rosenfeld, "Peak detection using difference operators," *IEEE Trans. Pattern Analysis and Machine Intelligence*, vol. PAMI-1, pp. 317–325, July 1979.

[7] J. F. Canny, "A computational approach to edge detection," *IEEE Trans. Pattern Analysis and Machine Intelligence*, vol. 8, pp. 679–698, November 1986.

[8] R. Bates and M. McDonnell, *Image Restoration and Reconstruction*. Clarendon Press, Oxford, 1986.

[9] W. Blass and G. Halsey, *Deconvolution of Absorption Spectra*. Academic Press, New York, 1981.

[10] W. H. Press, B. P. Flannery, S. A. Teukolsky, and W. T. Vetterling, *Numerical Recipes in C: The Art of Scientific Computing*. Cambridge University Press, 1988.

[11] M. Bertero and *et al*, "Three dimensional image restoration and super-resolution in fluorescence confocal microscopy," *J. Microscopy*, vol. 157, pp. 3–20, 1989.

[12] B. Frieden, "Image enhancement and restoration," in *Picture Processing and Digital Filtering* (T. Huang, ed.), Springer-Verlag, New York, 1979.

[13] P. Jansson, R. Hunt, and E. Plyler, "Resolution enhancement of spectra," *J. Opt. Soc. Am. A*, vol. 60, no. 2, pp. 596–599, 1970.

[14] R.O.Duda and P. Hart, *Pattern classification and scene analysis*. John Wiley and Sons, 1973.

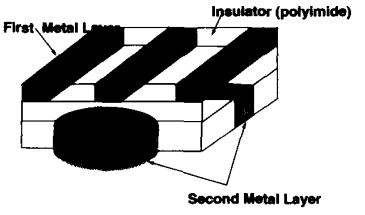

Figure 1: A schematic of the part to be inspected

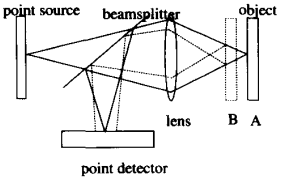

Figure 2: Imaging of the object using a confocal microscope. At position A the object is in focus, while at B it is defocused.

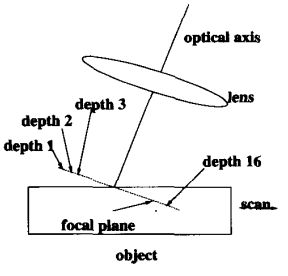

Figure 3: Illustrating the principle of tilted scanning

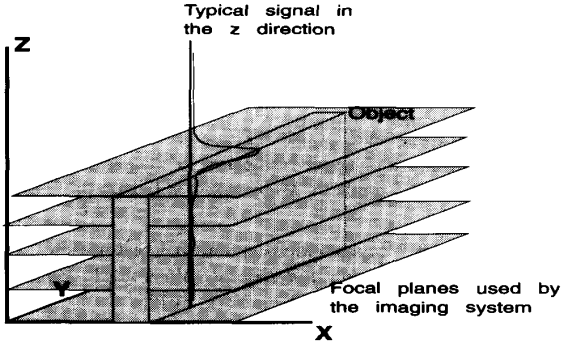

Figure 4: Numerous confocal image slices are stacked along the z-direction, which is parallel to the optical axis. The object being imaged is a thick metal line, whose top surface causes a peak in the intensity signal measured along the z axis.

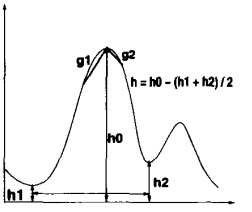

Figure 5: Peaks and valleys are identified through changes in the sign of the gradient. The height of a peak is defined to be the average height above the two neighboring valleys (minima).

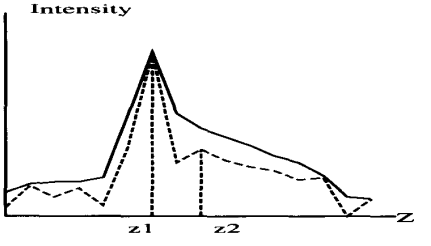

Figure 6: This figure shows the signal resulting from two surfaces at heights z_1 and z_2. The curve in solid lines represents the original signal. Note that the surfaces at z_1 and z_2 are close enough for their responses to overlap. This causes the original signal to contain only one peak. The result after applying deconvolution (Wiener filtering) is shown in dashed lines. Note that we have now resolved the two peaks at z_1 and z_2.

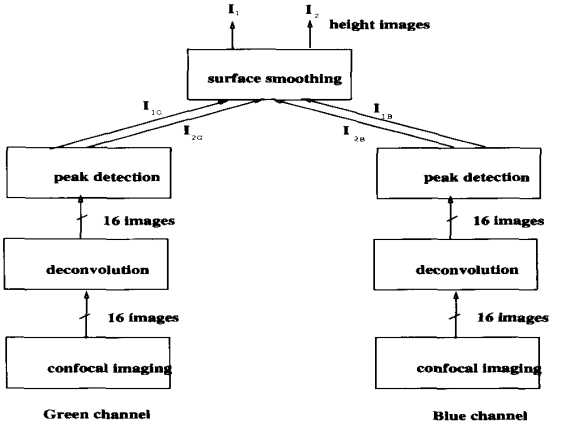

Figure 7: The block diagram of the system with the various processing stages shown. The objective of the process is to obtain two height images that can be used for further evaluation

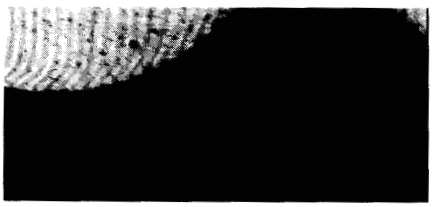

Figure 8: This figures shows interference fringes due to a thin polyimide film. The polyimide film covers the entire image. The circular region to the upper left is a metal surface. The interference between the metal and polyimide gives rise to the fringes.

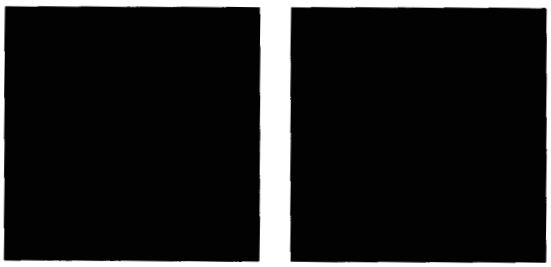

Figure 9: A set of confocal images. Each confocal image is of size 256x128 pixels. The images in figure (a) and (b) are of size 512x512, and each contains eight confocal images. The first eight images are shown in (a) and the next eight images are shown in (b). The sequencing is left to right and top to bottom.

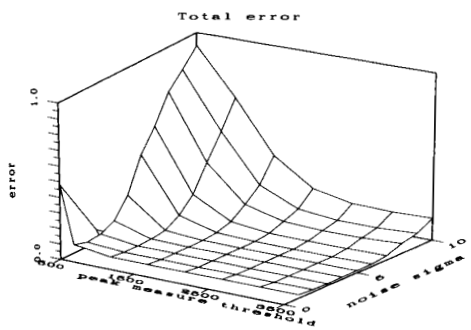

Figure 10: Error measurements to determine the global operating region

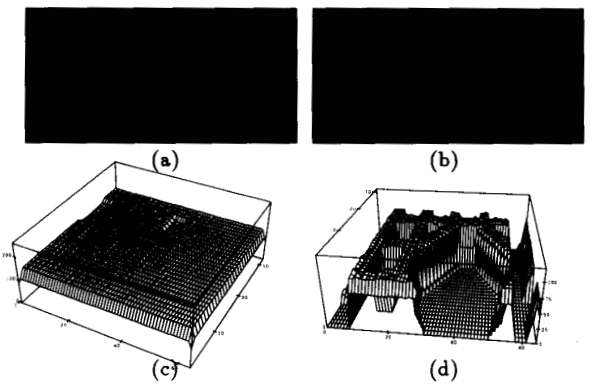

Figure 11: The result of applying Wiener filtering followed by peak detection and smoothing. Height is encoded via intensity. (a) The upper height image; (b) The lower height image. (c) and (d): A wireframe plot of the surfaces.

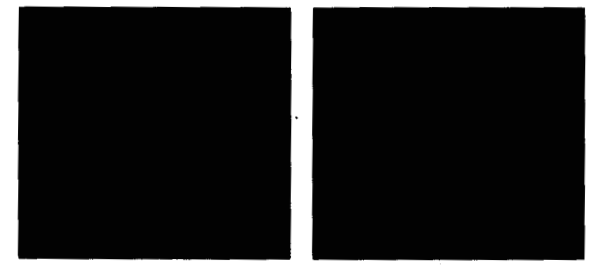

Figure 12: A set of confocal images of metal lines.

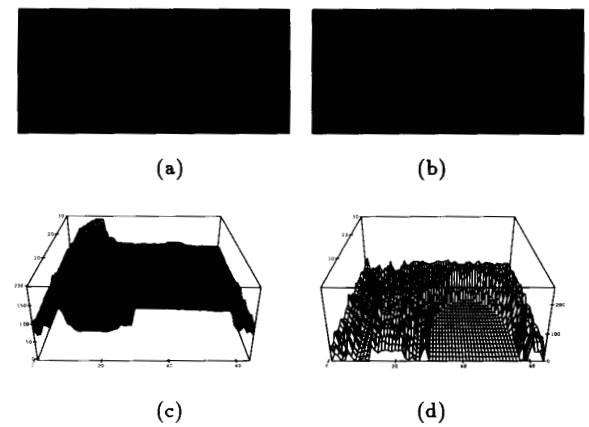

Figure 13: (a) The upper height image; (b) The lower height image. The heights are displayed using a wireframe model in (c) and (d).